

Search for the standard model Higgs boson in e^+e^- interactions at $\sqrt{s} = 189$ GeV

M. Acciarri, P. Achard, O. Adriani, M. Aguilar-Benitez, J. Alcaraz, G. Alemanni, J. Allaby, A. Aloisio, M G. Alviggi, G. Ambrosi, et al.

► **To cite this version:**

M. Acciarri, P. Achard, O. Adriani, M. Aguilar-Benitez, J. Alcaraz, et al.. Search for the standard model Higgs boson in e^+e^- interactions at $\sqrt{s} = 189$ GeV. Physics Letters B, Elsevier, 1999, 461, pp.376-386. 10.1016/S0370-2693(99)00853-9 . in2p3-00003674

HAL Id: in2p3-00003674

<http://hal.in2p3.fr/in2p3-00003674>

Submitted on 4 Oct 1999

HAL is a multi-disciplinary open access archive for the deposit and dissemination of scientific research documents, whether they are published or not. The documents may come from teaching and research institutions in France or abroad, or from public or private research centers.

L'archive ouverte pluridisciplinaire **HAL**, est destinée au dépôt et à la diffusion de documents scientifiques de niveau recherche, publiés ou non, émanant des établissements d'enseignement et de recherche français ou étrangers, des laboratoires publics ou privés.

**Search for the Standard Model Higgs boson
in e^+e^- interactions at $\sqrt{s} = 189$ GeV**

L3 Collaboration

Abstract

A search for the Standard Model Higgs boson is carried out on 176.4 pb^{-1} of data collected by the L3 detector at a center-of-mass energy of 189 GeV. The data are consistent with the expectations of Standard Model processes and no evidence of a Higgs signal is observed. Combining the results of this search with those at lower center-of-mass energies, a lower limit on the mass of the Standard Model Higgs boson of 95.3 GeV is set at the 95% confidence level.

Submitted to *Phys. Lett. B*

1 Introduction

In the Standard Model [1], a single Higgs doublet [2] gives rise to a neutral scalar, the Higgs boson, with a mass, m_H , that is a free parameter of the theory. Searches in e^+e^- collisions for the Standard Model Higgs boson have been reported up to center-of-mass energies of 183 GeV by L3 [3] and other experiments [4]. No evidence of a signal has been found and a combined lower limit of 89.7 GeV [5] is set at the 95% confidence level. In this letter, the results of a Higgs search performed on the data sample collected by L3 at $\sqrt{s} = 189$ GeV are reported, significantly extending the accessible range of m_H .

The dominant Higgs production mode,

$$e^+e^- \rightarrow Z^* \rightarrow HZ,$$

as well as the smaller production processes of W^+W^- and ZZ fusion, are considered. All significant signal decay modes are considered in the search. Four-fermion final states from W - and Z -pair production, as well as $e^+e^- \rightarrow q\bar{q}$, make up the largest sources of background.

2 Data and Monte Carlo samples

The data were collected using the L3 detector [6] at LEP during 1998. The integrated luminosity is 176.4 pb^{-1} at an average center-of-mass energy of 188.6 GeV.

Higgs production cross sections and branching ratios are calculated using the HZHA generator [7], whereas for the efficiency studies, Monte Carlo samples of Higgs events are generated using PYTHIA [8]. Standard Model background estimates are made with the following Monte Carlo programs: PYTHIA ($e^+e^- \rightarrow q\bar{q}(\gamma)$), KORALW [9] ($e^+e^- \rightarrow W^+W^-$), KORALZ [10] ($e^+e^- \rightarrow \tau^+\tau^-$), PYTHIA and PHOJET [11] ($e^+e^- \rightarrow e^+e^-q\bar{q}$), EXCALIBUR [12] ($e^+e^- \rightarrow f\bar{f}f'\bar{f}'$) and PYTHIA and EXCALIBUR ($e^+e^- \rightarrow Ze^+e^-$). The number of simulated events for the most important background channels is at least 100 times the number of collected data events for such processes, while the number of signal events is at least 300 times the number expected to be observed in the data with this integrated luminosity.

The response of the L3 detector is simulated using the GEANT 3.15 program [13], taking into account the effects of multiple scattering, energy loss and showering in the detector. Hadronic interactions in the detector are modeled using the GHEISHA program [14].

3 Analysis procedures

The search procedure is dictated by the four event topologies representing approximately 98% of the HZ decay modes: $q\bar{q}q\bar{q}$, $q\bar{q}\nu\bar{\nu}$, $q\bar{q}\ell^+\ell^-$ ($\ell = e, \mu, \tau$) and $\tau^+\tau^-q\bar{q}$. With the exception of $HZ \rightarrow \tau^+\tau^-q\bar{q}$, the analyses for each channel are optimized for $H \rightarrow b\bar{b}$, since this represents about 85% of the Higgs branching fraction in the mass range of interest. However, the efficiencies for the smaller contributions from $H \rightarrow c\bar{c}, gg$ are also considered.

The analyses for all the channels are performed in three stages. First, a high multiplicity hadronic event selection is applied, greatly reducing the large background from two-photon processes, while at the same time maintaining a high efficiency for the Higgs signal over a broad range of masses. Second, a tighter set of cuts specific to the topology in question is used to further enrich the sample of events while still maintaining signal efficiencies on the order of 50%. Finally, a discriminating variable is built for each analysis. These discriminants include

the results of a kinematic fit of the event, imposing 4-momentum conservation, and depend on the mass hypothesis value, m_H . The spectra of the discriminants are computed for the observed data and the Monte Carlo backgrounds and signals at each value of m_H considered, in the range $50 \text{ GeV} \leq m_H \leq 100 \text{ GeV}$.

The b-tagging variable, used to identify b quarks, plays a major role in the computation of the final discriminant. A neural network [15, 16] is used to calculate the b-tag for each hadronic jet from the three-dimensional decay lengths, semileptonic information and jet-shape variables. The b-tag variable used for the entire event is a combination of the individual jet-tag probabilities.

3.1 The $HZ \rightarrow b\bar{b}q\bar{q}$ channel

Events from this channel usually consist of four jets, two of which contain b hadrons, while the other two have a mass consistent with the Z mass. Standard Model processes which mimic these events are typically four-jet final states from $q\bar{q}$ with hard gluons, W^+W^- and ZZ events, especially those where one of the Z bosons decayed into b quarks.

Two independent analyses of this channel are performed, a neural network approach and a cut-based likelihood analysis. The cut-based analysis is the primary one used in this channel. The neural network analysis achieves similar performance and a description of the analysis technique can be found in Reference [3].

First, a preselection designed to accept high multiplicity hadronic events is applied by requiring at least 15 charged tracks and 20 calorimetric clusters. The visible energy, E_{vis} , must be between $0.6\sqrt{s}$ and $1.4\sqrt{s}$. The missing energy parallel and perpendicular to the beam direction has to be less than $0.3E_{\text{vis}}$. Finally, the energy of the most energetic photon or lepton must be less than 65 GeV.

At this stage, all the events passing the preselection are forced to have four jets using the DURHAM [17] clustering algorithm and a kinematic fit requiring 4-momentum conservation is performed. An automated procedure [15, 18] is used to optimize the selection criteria, which differentiates the Higgs signal from background based mainly on kinematic differences and large b-tag values. The cuts chosen by the optimizer, which do not depend on the m_H hypothesis, are as follows. To reject gluonic jets in $q\bar{q}$ events, the dijet masses must be between $0.13\sqrt{s}$ and $0.63\sqrt{s}$; the minimum jet energy must be larger than $0.14\sqrt{s}$ and the maximum energy difference between any two jets must be less than $0.22\sqrt{s}$. To enhance the four-jet nature of the events, the Y_{cut} parameter in the DURHAM scheme where the event goes from a three-jet to a four-jet topology, Y_{34}^D , is required to be larger than 0.0086. Finally, there must be at least 22 charged tracks. As in previous publications [18], the χ^2 -probability that depends on m_H and m_Z is used to quantify the consistency of the event with a given m_H hypothesis. A loose cut is placed on this variable, but more importantly, it is used along with the b-tag to calculate the mass-dependent final discriminant.

At this point, 682 events remain in the data and 703 in the Monte Carlo background, with 85% of these from W^+W^- events. These four-jet W^+W^- events are characterized by their low b-tag values and the consistency of the dijet masses with m_W . With this in mind, the optimizer splits the surviving events into high purity and low purity samples using a sliding cut on the reconstructed dijet mass, M_{eq}^{5C} , from a kinematic fit assuming the five constraints (5C) of 4-momentum conservation and equal masses for the two dijet systems. If $M_{\text{eq}}^{5C} > 0.74m_H + 21.7 \text{ GeV}$, then the event is placed into the high purity category, otherwise it is placed into the low purity category. The low purity sample contains most of the properly

reconstructed W^+W^- events, isolating a large component of the dominant background. In the high purity sample, the optimizer chooses b-tag values to be larger than 0.09, while in the low purity sample the cut is 0.41. The b-tag spectra for these two samples are shown in Figures 1(a) and 1(b).

After the final set of cuts, the high purity category contains 26 candidates with 31.0 expected from Standard Model processes and a signal efficiency of 28% for $HZ \rightarrow b\bar{b}q\bar{q}$ with $m_H = 95$ GeV. The low purity category has 263 candidates, 239 expected background events and a 34% signal efficiency.

Once the final set of cuts has been applied, the weighted probability [15,18] that an event is consistent with the background distributions of both the b-tag and the mass variable is calculated. Since the weighted combination depends on the mass hypothesis, m_H , the distributions of this discriminant are calculated for each test mass, an example of which can be found in Figures 1(c) and 1(d). The observed candidates in the $HZ \rightarrow b\bar{b}q\bar{q}$ channel are consistent with the Monte Carlo background predictions.

3.2 The $HZ \rightarrow b\bar{b}\nu\bar{\nu}$ channel

This channel is characterized by two acoplanar jets and large missing transverse energy. The missing mass is consistent with m_Z and the hadronic jets typically contain b hadrons.

Two independent analyses of this channel are carried out, a neural network and a cut-based likelihood analysis. The analyses have similar performance and lead to consistent results. In this letter, the neural network analysis is described.

First, high multiplicity hadronic events with more than 3 charged tracks and at least 15 calorimetric energy clusters are selected. Using the DURHAM algorithm, all energy clusters in the event are combined to form two hadronic jets. The reconstructed mass of each of these jets must exceed 40 GeV. These cuts reduce contributions from purely leptonic two-fermion final states, as well as two-photon interactions, while keeping a significant fraction of hadronic events from $e^+e^- \rightarrow q\bar{q}(\gamma)$ and W-pair production. These latter contributions are further reduced by requiring the visible mass to be less than 120 GeV and the mass recoiling against the hadronic system to lie between 50 GeV and 130 GeV.

Events from $e^+e^- \rightarrow q\bar{q}(\gamma)$ are further suppressed with missing-energy requirements. The missing energy transverse to the beam axis should be greater than 5 GeV, the missing momentum vector must be at least 16° from this axis and the longitudinal missing energy is required to be less than $0.7\sqrt{s}$. The opening angle between the two jets has to be greater than 69° and the angle between the jet-jet plane and the beam-axis must be greater than 3° . The energy in the forward luminosity calorimeter is required to be smaller than 15 GeV. In addition, the event b-tag must be larger than 0.5. The b-tag spectra for data and Monte Carlo are shown in Figure 2(a). After this final set of cuts, there remain 109 data events, with 116 expected from Standard Model processes and an efficiency of 62% for $HZ \rightarrow b\bar{b}\nu\bar{\nu}$ with $m_H = 95$ GeV.

A mass-independent neural network [3] is then used to further separate the signal from background. A kinematic fit imposing 4-momentum conservation and requiring the missing mass to be m_Z is performed, yielding the hadronic mass, M_H^{5C} . The neural network output is shown in Figure 2(b), and the distribution of M_H^{5C} is shown in Figure 2(c). The M_H^{5C} mass is combined with the neural network output to form the purity variable [3]. This purity variable plays the role of the final discriminant in the $HZ \rightarrow b\bar{b}\nu\bar{\nu}$ analysis and is shown in Figure 2(d) for the mass hypothesis $m_H = 95$ GeV. The observed data in the $HZ \rightarrow b\bar{b}\nu\bar{\nu}$ analysis are compatible with the Monte Carlo background expectations.

3.3 The $\text{HZ} \rightarrow \text{b}\bar{\text{b}}\text{e}^+\text{e}^-$ and $\text{HZ} \rightarrow \text{b}\bar{\text{b}}\mu^+\mu^-$ channels

The signatures for $\text{HZ} \rightarrow \text{b}\bar{\text{b}}\text{e}^+\text{e}^-$ and $\text{HZ} \rightarrow \text{b}\bar{\text{b}}\mu^+\mu^-$ are a pair of high energy electrons or muons, with an invariant mass near m_Z , and two hadronic b jets.

A hadronic event selection is applied requiring at least 5 charged tracks, 15 calorimetric clusters and two well identified electrons or muons. The visible energy must be larger than $0.7\sqrt{s}$ for the electron analysis and $0.4\sqrt{s}$ for the muon analysis. In the $\text{HZ} \rightarrow \text{b}\bar{\text{b}}\text{e}^+\text{e}^-$ analysis, the electron pair must have an opening angle greater than 100° , while for $\text{HZ} \rightarrow \text{b}\bar{\text{b}}\mu^+\mu^-$, the muon pair must have an opening angle greater than 90° . In addition, there must be less than $0.4\sqrt{s}$ of missing energy perpendicular to the beam direction. Both analyses must have values of Y_{34}^{D} larger than 0.0009. Finally, the invariant mass of the leptonic system after a kinematic fit imposing 4-momentum conservation must be between 60 GeV and 110 GeV for the electrons and 50 GeV and 125 GeV for the muons. After this final set of cuts, the number of remaining candidates in the electron channel is 15, with 13.2 expected from Standard Model backgrounds and a signal efficiency for $\text{HZ} \rightarrow \text{b}\bar{\text{b}}\text{e}^+\text{e}^-$ of 77% for $m_{\text{H}} = 95$ GeV. The corresponding numbers for the muon channel are 5 candidates with 5.5 background expected and a signal efficiency for $\text{HZ} \rightarrow \text{b}\bar{\text{b}}\mu^+\mu^-$ of 57%.

After performing a kinematic fit requiring 4-momentum conservation and constraining the mass of the lepton pair to m_Z , the mass of the jet-jet system is combined with the b-tags of jet 1 and jet 2. For each event class j (ZZ , W^+W^- , $\text{q}\bar{\text{q}}$, Ze^+e^- , HZ), a probability density function f_j^i is constructed, where i denotes the b-tag of jet 1, the b-tag of jet 2, or the dijet mass. The probability of an event to belong to class j , based solely on the value of the variable i , is then defined as

$$p_j^i = \frac{f_j^i}{\sum_k f_k^i}. \quad (1)$$

Finally, the probabilities for the individual variables are combined by calculating the likelihood that the event belongs to the signal class HZ :

$$F_{\text{HZ}} = \frac{\prod_i p_{\text{HZ}}^i}{\sum_k \prod_i p_k^i}. \quad (2)$$

The spectra for this final discriminant, F_{HZ} , in the electron and muon channels are shown in Figures 3(a) and 3(b) for the data, background and a 95 GeV Higgs signal. The observed candidates are consistent with the Monte Carlo background predictions.

3.4 The $\text{HZ} \rightarrow \text{b}\bar{\text{b}}\tau^+\tau^-$ and $\text{HZ} \rightarrow \tau^+\tau^-\text{q}\bar{\text{q}}$ channels

The $\text{HZ} \rightarrow \text{b}\bar{\text{b}}\tau^+\tau^-$ and $\text{HZ} \rightarrow \tau^+\tau^-\text{q}\bar{\text{q}}$ final states are very similar and can be distinguished only with mass and b-tag information. The semileptonic W- and Z-pair decays are the most significant background sources.

Two inclusive selections are performed, one based on a tau identification (particle-based selection) and one relying more on the event kinematics (jet-based selection). Events are accepted if they pass either of the two selections.

First, a common preselection is applied, requiring more than 4 charged tracks, more than 14 clusters and a visible energy of more than $0.4\sqrt{s}$. The events are subject to the DURHAM algorithm, keeping only those with Y_{34}^{D} larger than 0.0025. Background from $\text{e}^+\text{e}^- \rightarrow \text{q}\bar{\text{q}}(\gamma)$ is reduced by rejecting events containing photons with energies greater than 40 GeV. The

contribution of $W^+W^- \rightarrow q\bar{q}\ell\nu$ ($\ell = e, \mu$) is reduced by requiring the energy of electrons and muons to be smaller than 40 GeV.

In the particle-based selection, tau leptons are identified via their decay into electrons or muons, or as an isolated low-multiplicity jet with 1 or 3 tracks and unit charge. In the jet-based selection, the event is forced into four jets using the DURHAM algorithm. Two of the jets must each have less than 4 tracks. These jets are considered as tau candidates, but at least one of them must coincide with a tau candidate defined in the particle-based selection within a 3° cone. Both taus must be separated from the hadronic jets by at least 25° . Background contamination from fully hadronic W^+W^- decays is reduced by rejecting events where both taus decay into 3 charged particles and by requiring the visible energy to be smaller than $0.95\sqrt{s}$ for the particle-based and smaller than $0.9\sqrt{s}$ for the jet-based selection. Moreover, in the jet-based selection, the polar angle of the missing momentum vector, Θ_{miss} , must satisfy $|\cos \Theta_{\text{miss}}| \leq 0.95$ in order to reduce $q\bar{q}(\gamma)$ contamination.

The invariant masses of the tau-tau and the jet-jet systems are obtained from a kinematic fit which imposes 4-momentum conservation. An event qualifies for the $HZ \rightarrow b\bar{b}\tau^+\tau^-$ channel if the invariant mass of the tau-tau system is consistent with the mass of the Z boson by lying between 70 GeV and 125 GeV. Similarly, an event qualifies for the $HZ \rightarrow \tau^+\tau^-q\bar{q}$ channel if the jet-jet mass fulfills this same requirement. Furthermore, the opening angle of the particles or jets assigned to the Higgs boson must be larger than 70° and those assigned to the Z must be at least 100° apart. Cross-efficiencies on the $HZ \rightarrow b\bar{b}e^+e^-$ and the $HZ \rightarrow b\bar{b}\mu^+\mu^-$ channels (up to 3%) are taken into account by rejecting events which were already selected in those analyses. In total, 12 candidate events are selected, with 17.1 events expected from Standard Model background processes passing either of the tau selections, and an efficiency of 30% for both $HZ \rightarrow b\bar{b}\tau^+\tau^-$ and $HZ \rightarrow \tau^+\tau^-q\bar{q}$ at $m_H = 95$ GeV.

The final discriminant for the $HZ \rightarrow b\bar{b}\tau^+\tau^-$ channel is defined similarly to the likelihood used in the $HZ \rightarrow b\bar{b}e^+e^-$ and $HZ \rightarrow b\bar{b}\mu^+\mu^-$ analyses, using Equations 1 and 2. For the $HZ \rightarrow \tau^+\tau^-q\bar{q}$ channel, the mass distribution of the tau pair, after constraining the invariant mass of the jets to m_Z , is used as the final discriminant. Events that pass both decay hypotheses are placed into the channel with the larger value of the likelihood, F_{HZ} , defined in Equation 2. Distributions of these discriminants can be found in Figures 3(c) and 3(d) for data, background and a 95 GeV Higgs signal. No evidence of a signal is seen in either of the tau channels.

4 Combined results

The results of all the previously described analyses are combined in this section. For illustrative purposes, in Figure 4(a) the reconstructed Higgs mass is shown for a sample of signal-like events selected by the analyses after making a mass-independent requirement, such as a large b-tag value or large neural network output. In Figures 4(b) and 4(c), the results of the mass-dependent selections are illustrated by plotting the reconstructed Higgs mass for events with large discriminant values (signal-over-background ratio greater than 0.25) for the 90 GeV and 95 GeV mass hypotheses. No evidence of a signal is present in any of the analyses and a global confidence level (CL) on the absence of a signal is calculated from the spectra of final discriminants from all the analyses in a scan over m_H from 50 GeV to 100 GeV. The CL is calculated using the techniques of References [16, 19], which also allow correlated and statistical errors to be easily accounted for in the computation of CL.

The statistical and systematic errors on the signal and background are considered using the

same procedure as previous Standard Model Higgs searches by L3 [3,16]. The overall systematic error is estimated at 10% on the number of background events and 5% on the number of signal events. The statistical error on the background from the finite number of generated Monte Carlo events is larger, but is uncorrelated from bin to bin in the final discriminant distributions, and has little effect on the CL. Bins with a signal-over-background ratio smaller than 0.05 are not considered during the calculation of CL. This cut was chosen to maximize the average CL, as calculated from a large number of Monte Carlo experiments, thereby minimizing the degradation of the result due to these systematic and statistical errors for this integrated luminosity and center-of-mass energy. The results of all the analyses after such a signal-over-background cut are summarized in Table 1 for the data, Monte Carlo background and signal. The number of signal events includes cross-efficiencies from other channels, fusion processes and charm and gluonic Higgs decays.

The measured value of CL as a function of the Standard Model Higgs boson mass, in the range $85 \leq m_H \leq 100$ GeV, is shown in Figure 5(a), along with the median of the CL distribution as calculated from a large sample of Monte Carlo experiments assuming a background-only hypothesis. The number of Higgs events expected to be observed, as a function of m_H , and the number of excluded signal events at the 95% CL are shown in Figure 5(b). The results of previous L3 Standard Model Higgs searches at lower center-of-mass energies [3,16,20] have been included in the calculation of these confidence levels. Values of m_H from 50 GeV to 85 GeV are excluded to greater than the 99.999% confidence level by the 189 GeV data alone and have been previously excluded by the L3 analyses at lower center-of-mass energies. The median CL represents the sensitivity of the global analysis and is equal to 95% at $m_H = 94.8$ GeV, while the average CL is 95% at 92.7 GeV. Where the observed CL falls below 95%, the probability to observe a higher limit is 37%.

The lower limit on the Standard Model Higgs boson mass is set at

$$m_H > 95.3 \text{ GeV at } 95\% \text{ CL.}$$

This new lower limit improves upon and supersedes our previously published results.

Acknowledgments

We acknowledge the efforts of the engineers and technicians who have participated in the construction and maintenance of L3 and express our gratitude to the CERN accelerator divisions for the superb performance of LEP.

References

- [1] S. L. Glashow, Nucl. Phys. **22** (1961) 579.
S. Weinberg, Phys. Rev. Lett. **19** (1967) 1264.
A. Salam, "Weak and Electromagnetic Interactions", in *Elementary Particle Theory*, edited by N. Svartholm, page 367, Stockholm, 1968, Almqvist and Wiksell.
- [2] P. W. Higgs, Phys. Lett. **12** (1964) 132.
F. Englert and R. Brout, Phys. Rev. Lett. **13** (1964) 321.
G. S. Guralnik *et al.*, Phys. Rev. Lett. **13** (1964) 585.

- [3] L3 Collaboration, M. Acciarri *et al.*, Phys. Lett. **B 431** (1998) 437.
- [4] OPAL Collaboration, G. Abbiendi *et al.*, Eur. Phys. Jo. **C 7** (1999) 407.
DELPHI Collaboration, P. Abreu *et al.*, “Search for neutral Higgs bosons in e^+e^- collisions at $\sqrt{s} = 183$ GeV”, Preprint EP/99-006, CERN, 1999, Accepted for publication by E. Phys. J. **C**.
ALEPH Collaboration, R. Barate *et al.*, Phys. Lett. **B 447** (1999) 336.
- [5] LEP Working Group for Higgs Boson Searches *et al.*, “Limits on Higgs boson masses from combining the data of the four LEP experiments at $\sqrt{s} \leq 183$ GeV”, CERN-EP/99-060, 1999.
- [6] L3 Collaboration, B. Adeva *et al.*, Nucl. Inst. Meth. **A 289** (1990) 35.
J. A. Bakken *et al.*, Nucl. Inst. Meth. **A 275** (1989) 81.
O. Adriani *et al.*, Nucl. Inst. Meth. **A 302** (1991) 53.
B. Adeva *et al.*, Nucl. Inst. Meth. **A 323** (1992) 109.
K. Deiters *et al.*, Nucl. Inst. Meth. **A 323** (1992) 162.
M. Chemarin *et al.*, Nucl. Inst. Meth. **A 349** (1994) 345.
M. Acciarri *et al.*, Nucl. Inst. Meth. **A 351** (1994) 300.
G. Basti *et al.*, Nucl. Inst. Meth. **A 374** (1996) 293.
A. Adam *et al.*, Nucl. Inst. Meth. **A 383** (1996) 342.
- [7] G. Altarelli, T. Sjöstrand, and F. Zwirner, editors, *Physics at LEP2*, Geneva, Switzerland, 1996, CERN, CERN 96-01.
- [8] T. Sjöstrand, “PYTHIA”, Preprint TH/93-7112, CERN, 1993, Revised August 1995.
T. Sjöstrand, Comp. Phys. Comm. **82** (1994) 74.
- [9] M. Skrzypek *et al.*, Comp. Phys. Comm. **94** (1996) 216.
M. Skrzypek *et al.*, Phys. Lett. **B 372** (1996) 289.
- [10] S. Jadach, B. F. L. Ward, and Z. Wąs, Comp. Phys. Comm. **66** (1991) 276.
- [11] R. Engel, Z. Phys. **C 66** (1995) 203.
R. Engel, J. Ranft, and S. Roesler, Phys. Rev. **D 52** (1995) 1459.
- [12] F. A. Berends, R. Pittau, and R. Kleiss, Comp. Phys. Comm. **85** (1995) 437.
- [13] R. Brun *et al.*, “GEANT 3”, CERN DD/EE/84-1, Revised 1987.
- [14] H. Fesefeldt, “GHEISHA”, Preprint PITHA 85/02, RWTH Aachen, 1985.
- [15] A. Dominguez, *Search for Neutral Higgs Bosons in e^+e^- Interactions at Center-of-Mass Energies Between 130 GeV and 183 GeV*, PhD thesis, UCSD, 1998, <http://hep.ucsd.edu/thesis/aaron.html>.
- [16] L3 Collaboration, M. Acciarri *et al.*, Phys. Lett. **B 411** (1997) 373.

- [17] S. Bethke *et al.*, Nucl. Phys. **B 370** (1992) 310.
- [18] L3 Collaboration, M. Acciarri *et al.*, Phys. Lett. **B 436** (1998) 389.
- [19] A. Favara and M. Pieri, “Confidence Level Estimation and Analysis Optimization”, Preprint, INFN University of Florence, 1997, DFF-278-4-1997.
- [20] L3 Collaboration, M. Acciarri *et al.*, Phys. Lett. **B 385** (1996) 454.

The L3 Collaboration:

M. Acciarri,²⁵ P. Achard,¹⁸ O. Adriani,¹⁵ M. Aguilar-Benitez,²⁴ J. Alcaraz,²⁴ G. Alemanni,²¹ J. Allaby,¹⁶ A. Aloisio,²⁷ M. G. Alvigi,²⁷ G. Ambrosi,¹⁸ H. Anderhub,⁴⁶ V. P. Andreev,^{6,35} T. Angelescu,¹² F. Anselmo,⁹ A. Arefiev,²⁶ T. Azemoon,³ T. Aziz,¹⁰ P. Bagnaia,³⁴ L. Baksay,⁴¹ A. Balandras,⁴ R. C. Ball,³ S. Banerjee,¹⁰ Sw. Banerjee,¹⁰ A. Barczyk,^{46,44} R. Barillere,¹⁶ L. Barone,³⁴ P. Bartalini,²¹ M. Basile,⁹ R. Battiston,³¹ A. Bay,²¹ F. Becattini,¹⁵ U. Becker,¹⁴ F. Behner,⁴⁶ J. Berdugo,²⁴ P. Berges,¹⁴ B. Bertucci,³¹ B. L. Betev,⁴⁶ S. Bhattacharya,¹⁰ M. Biasini,³¹ A. Biland,⁴⁶ J. J. Blaising,⁴ S. C. Blyth,³² G. J. Bobbink,² A. Böhm,¹ L. Boldizsar,¹³ B. Borgia,³⁴ D. Bourilkov,⁴⁶ M. Bourquin,¹⁸ S. Braccini,¹⁸ J. G. Branson,³⁷ V. Brigljevic,⁴⁶ F. Brochu,⁴ A. Buffini,¹⁵ A. Buijs,⁴² J. D. Burger,¹⁴ W. J. Burger,³¹ J. Busenitz,⁴¹ A. Button,³ X. D. Cai,¹⁴ M. Campanelli,⁴⁶ M. Capell,¹⁴ G. Cara Romeo,⁹ G. Carlino,²⁷ A. M. Cartacci,¹⁵ J. Casaus,²⁴ G. Castellini,¹⁵ F. Cavallari,³⁴ N. Cavallo,²⁷ C. Cecchi,¹⁸ M. Cerrada,²⁴ F. Cesaroni,²² M. Chamizo,¹⁸ Y. H. Chang,⁴⁸ U. K. Chaturvedi,¹⁷ M. Chemarin,²³ A. Chen,⁴⁸ G. Chen,⁷ G. M. Chen,⁷ H. F. Chen,¹⁹ H. S. Chen,⁷ X. Chereau,⁴ G. Chiefari,²⁷ L. Cifarelli,³⁶ F. Cindolo,⁹ C. Civinini,¹⁵ I. Clare,¹⁴ R. Clare,¹⁴ G. Coignet,⁴ A. P. Colijn,² N. Colino,²⁴ S. Costantini,⁸ F. Cotorobai,¹² B. Cozzoni,⁹ B. de la Cruz,²⁴ A. Csilling,¹³ S. Cucciarelli,³¹ T. S. Dai,¹⁴ J. A. van Dalen,²⁹ R. D' Alessandro,¹⁵ R. de Asmundis,²⁷ P. Deglon,¹⁸ A. Degré,⁴ K. Deiters,⁴⁴ D. della Volpe,²⁷ P. Denes,³³ F. De Notaristefani,³⁴ A. De Salvo,⁴⁶ M. Diemoz,³⁴ D. van Dierendonck,² F. Di Lodovico,⁴⁶ C. Dionisi,³⁴ M. Dittmar,⁴⁶ A. Dominguez,³⁷ A. Doria,²⁷ M. T. Dova,^{17,‡} D. Duchesneau,⁴ D. Dufournand,⁴ P. Duinker,² I. Duran,³⁸ H. El Mamouni,²³ A. Engler,³² F. J. Eppling,¹⁴ F. C. Erne,² P. Extermann,¹⁸ M. Fabre,⁴⁴ R. Faccini,³⁴ M. A. Falagan,²⁴ S. Falciano,^{34,16} A. Favara,¹⁶ J. Fay,²³ O. Fedin,³⁵ M. Felcini,⁴⁶ T. Ferguson,³² F. Ferroni,³⁴ H. Fesefeldt,¹ E. Fiandrina,³¹ J. H. Field,¹⁸ F. Filthaut,¹⁶ P. H. Fisher,¹⁴ I. Fisk,³⁷ G. Forconi,¹⁴ L. Fredj,¹⁸ K. Freudenreich,⁴⁶ C. Furetta,²⁵ Yu. Galaktionov,^{26,14} S. N. Ganguli,¹⁰ P. Garcia-Abia,⁵ M. Gataullin,³⁰ S. S. Gau,¹¹ S. Gentile,^{34,16} N. Gheordanescu,¹² S. Giagu,³⁴ Z. F. Gong,¹⁹ G. Grenier,²³ O. Grimm,⁴⁶ M. W. Gruenewald,⁸ R. van Gulik,² V. K. Gupta,³³ A. Gurtu,¹⁰ L. J. Gutay,⁴³ D. Haas,⁵ A. Hasan,²⁸ D. Hatzifotiadou,⁹ T. Hebbeker,⁸ A. Hervé,⁶ P. Hidas,¹³ J. Hirschfelder,³² H. Hofer,⁴⁶ G. Holzner,⁴⁶ H. Hoorani,³² S. R. Hou,⁴⁸ I. Iashvili,⁴⁵ B. N. Jin,⁷ L. W. Jones,³ P. de Jong,² I. Josa-Mutuberría,²⁴ R. A. Khan,¹⁷ D. Kamrad,⁴⁵ M. Kaur,^{17,◇} M. N. Kienzle-Focacci,¹⁸ D. Kim,³⁴ D. H. Kim,⁴⁰ J. K. Kim,⁴⁰ S. C. Kim,⁴⁰ J. Kirkby,¹⁶ D. Kiss,¹³ W. Kittel,²⁹ A. Klimentov,^{14,26} A. C. König,²⁹ A. Kopp,⁴⁵ I. Korolko,²⁶ V. Koutsenko,^{14,26} M. Kräber,⁴⁶ R. W. Kraemer,³² W. Krenz,¹ A. Kunin,^{14,26} P. Lacentre,^{45,‡,‡} P. Ladron de Guevara,²⁴ I. Laktineh,²³ G. Landi,¹⁵ K. Lassila-Perini,⁴⁶ P. Laurikainen,²⁰ A. Lavorato,³⁶ M. Lebeau,¹⁶ A. Lebedev,¹⁴ P. Lebrun,²³ P. Lecomte,⁴⁶ P. Lecoq,¹⁶ P. Le Coultre,⁴⁶ H. J. Lee,⁸ J. M. Le Goff,¹⁶ R. Leiste,⁴⁵ E. Leonardi,³⁴ P. Levchenko,³⁵ C. Li,¹⁹ C. H. Lin,⁴⁸ W. T. Lin,⁴⁸ F. L. Linde,² L. Lista,²⁷ Z. A. Liu,⁷ W. Lohmann,⁴⁵ E. Longo,³⁴ Y. S. Lu,⁷ K. Lübelmeyer,¹ C. Luci,^{16,34} D. Luckey,¹⁴ L. Lugnier,²³ L. Luminari,³⁴ W. Lusteremann,⁴⁶ W. G. Ma,¹⁹ M. Maity,¹⁰ L. Malgeri,¹⁶ A. Malinin,^{26,16} C. Mañá,²⁴ D. Mangeol,²⁹ P. Marchesini,⁴⁶ G. Marian,^{41,¶} J. P. Martin,²³ F. Marzano,³⁴ G. G. Massaro,² K. Mazumdar,¹⁰ R. R. McNeil,⁶ S. Mele,¹⁶ L. Merola,²⁷ M. Meschini,¹⁵ W. J. Metzger,²⁹ M. von der Mey,¹ D. Miganí,⁹ A. Mihul,¹² H. Milcent,¹⁸ G. Mirabelli,³⁴ J. Mnich,¹⁶ G. B. Mohanty,¹⁰ P. Molnar,⁸ B. Monteleon,^{15,†} T. Moulik,¹⁰ G. S. Muanza,²³ F. Muheim,¹⁸ A. J. M. Muijs,² M. Napolitano,²⁷ F. Nessi-Tedaldi,⁴⁶ H. Newman,³⁰ T. Niessen,¹ A. Nisati,³⁴ H. Nowak,⁴⁵ Y. D. Oh,⁴⁰ G. Organtini,³⁴ R. Ostonen,²⁰ C. Palomares,²⁴ D. Pandoulas,¹ S. Paoletti,^{34,16} P. Paolucci,²⁷ H. K. Park,³² I. H. Park,⁴⁰ G. Pascale,³⁴ G. Passaleva,¹⁶ S. Patricelli,²⁷ T. Paul,¹¹ M. Pauluzzi,³¹ C. Paus,¹⁶ F. Pauss,⁴⁶ D. Peach,¹⁶ M. Pedace,³⁴ Y. J. Pei,¹ S. Pensotti,²⁵ D. Perret-Gallix,⁴ B. Petersen,²⁹ D. Piccolo,²⁷ M. Pieri,¹⁵ P. A. Piroué,³³ E. Pistoiesi,²⁵ V. Plyaskin,²⁶ M. Pohl,⁴⁶ V. Pojidaev,^{26,15} H. Postema,¹⁴ J. Pothier,¹⁶ N. Produit,¹⁸ D. O. Prokofiev,⁴³ D. Prokofiev,³⁵ J. Quartieri,³⁶ G. Rahal-Callot,^{46,16} M. A. Rahaman,¹⁰ N. Raja,¹⁰ R. Ramelli,⁴⁶ P. G. Rancoita,²⁵ G. Raven,³⁷ P. Razis,²⁸ D. Ren,⁴⁶ M. Rescigno,³⁴ S. Reucroft,¹¹ T. van Rhee,⁴² S. Riemann,⁴⁵ K. Riles,³ A. Robohm,⁴⁶ J. Rodin,⁴¹ B. P. Roe,³ L. Romero,²⁴ A. Rosca,⁸ S. Rosier-Lees,⁴ J. A. Rubio,¹⁶ D. Ruschmeier,⁸ H. Rykaczewski,⁴⁶ S. Sarkar,³⁴ J. Salicio,¹⁶ E. Sanchez,¹⁶ M. P. Sanders,²⁹ M. E. Sarakinos,²⁰ C. Schäfer,¹ V. Schegelsky,³⁵ S. Schmidt-Kaerst,¹ D. Schmitz,¹ H. Schopper,⁴⁷ D. J. Schotanus,²⁹ J. Schwenke,¹ G. Schwering,¹ C. Sciacca,²⁷ D. Sciarrino,¹⁸ A. Seganti,⁹ L. Servoli,³¹ S. Shevchenko,³⁰ N. Shivarov,³⁹ V. Shoutko,²⁶ E. Shumilov,²⁶ A. Shvorob,³⁰ T. Siedenburger,¹ D. Son,⁴⁰ B. Smith,³² P. Spillantini,¹⁵ M. Steuer,¹⁴ D. P. Stickland,³³ A. Stone,⁶ H. Stone,^{33,†} B. Stoyanov,³⁹ A. Straessner,¹ K. Sudhakar,¹⁰ G. Sultanov,¹⁷ L. Z. Sun,¹⁹ H. Suter,⁴⁶ J. D. Swain,¹⁷ Z. Szillasi,^{41,¶} X. W. Tang,⁷ L. Tauscher,⁵ L. Taylor,¹¹ C. Timmermans,²⁹ Samuel C. C. Ting,¹⁴ S. M. Ting,¹⁴ S. C. Tonwar,¹⁰ J. Tóth,¹³ C. Tully,³³ K. L. Tung,⁷ Y. Uchida,¹⁴ J. Ulbricht,⁴⁶ E. Valente,³⁴ G. Vesztegombi,¹³ I. Vetlitsky,²⁶ D. Vicinanza,³⁶ G. Viertel,⁴⁶ S. Villa,¹¹ M. Vivargent,⁴ S. Vlachos,⁵ I. Vodopianov,³⁵ H. Vogel,³² H. Vogt,⁴⁵ I. Vorobiev,²⁶ A. A. Vorobyov,³⁵ A. Vorvolakos,²⁸ M. Wadhwa,⁵ W. Wallraff,¹ M. Wang,¹⁴ X. L. Wang,¹⁹ Z. M. Wang,¹⁹ A. Weber,¹ M. Weber,¹ P. Wienemann,¹ H. Wilkens,²⁹ S. X. Wu,¹⁴ S. Wynhoff,¹ L. Xia,³⁰ Z. Z. Xu,¹⁹ B. Z. Yang,¹⁹ C. G. Yang,⁷ H. J. Yang,⁷ M. Yang,⁷ J. B. Ye,¹⁹ S. C. Yeh,⁴⁹ An. Zalite,³⁵ Yu. Zalite,³⁵ Z. P. Zhang,¹⁹ G. Y. Zhu,⁷ R. Y. Zhu,³⁰ A. Zichichi,^{9,16,17} F. Ziegler,⁴⁵ G. Zilizi,^{41,¶} M. Zöller,¹

- 1 I. Physikalisches Institut, RWTH, D-52056 Aachen, FRG[§]
III. Physikalisches Institut, RWTH, D-52056 Aachen, FRG[§]
 - 2 National Institute for High Energy Physics, NIKHEF, and University of Amsterdam, NL-1009 DB Amsterdam, The Netherlands
 - 3 University of Michigan, Ann Arbor, MI 48109, USA
 - 4 Laboratoire d'Annecy-le-Vieux de Physique des Particules, LAPP, IN2P3-CNRS, BP 110, F-74941 Annecy-le-Vieux CEDEX, France
 - 5 Institute of Physics, University of Basel, CH-4056 Basel, Switzerland
 - 6 Louisiana State University, Baton Rouge, LA 70803, USA
 - 7 Institute of High Energy Physics, IHEP, 100039 Beijing, China[△]
 - 8 Humboldt University, D-10099 Berlin, FRG[§]
 - 9 University of Bologna and INFN-Sezione di Bologna, I-40126 Bologna, Italy
 - 10 Tata Institute of Fundamental Research, Bombay 400 005, India
 - 11 Northeastern University, Boston, MA 02115, USA
 - 12 Institute of Atomic Physics and University of Bucharest, R-76900 Bucharest, Romania
 - 13 Central Research Institute for Physics of the Hungarian Academy of Sciences, H-1525 Budapest 114, Hungary[‡]
 - 14 Massachusetts Institute of Technology, Cambridge, MA 02139, USA
 - 15 INFN Sezione di Firenze and University of Florence, I-50125 Florence, Italy
 - 16 European Laboratory for Particle Physics, CERN, CH-1211 Geneva 23, Switzerland
 - 17 World Laboratory, FBLJA Project, CH-1211 Geneva 23, Switzerland
 - 18 University of Geneva, CH-1211 Geneva 4, Switzerland
 - 19 Chinese University of Science and Technology, USTC, Hefei, Anhui 230 029, China[△]
 - 20 SEFT, Research Institute for High Energy Physics, P.O. Box 9, SF-00014 Helsinki, Finland
 - 21 University of Lausanne, CH-1015 Lausanne, Switzerland
 - 22 INFN-Sezione di Lecce and Università Degli Studi di Lecce, I-73100 Lecce, Italy
 - 23 Institut de Physique Nucléaire de Lyon, IN2P3-CNRS, Université Claude Bernard, F-69622 Villeurbanne, France
 - 24 Centro de Investigaciones Energéticas, Medioambientales y Tecnológicas, CIEMAT, E-28040 Madrid, Spain[‡]
 - 25 INFN-Sezione di Milano, I-20133 Milan, Italy
 - 26 Institute of Theoretical and Experimental Physics, ITEP, Moscow, Russia
 - 27 INFN-Sezione di Napoli and University of Naples, I-80125 Naples, Italy
 - 28 Department of Natural Sciences, University of Cyprus, Nicosia, Cyprus
 - 29 University of Nijmegen and NIKHEF, NL-6525 ED Nijmegen, The Netherlands
 - 30 California Institute of Technology, Pasadena, CA 91125, USA
 - 31 INFN-Sezione di Perugia and Università Degli Studi di Perugia, I-06100 Perugia, Italy
 - 32 Carnegie Mellon University, Pittsburgh, PA 15213, USA
 - 33 Princeton University, Princeton, NJ 08544, USA
 - 34 INFN-Sezione di Roma and University of Rome, "La Sapienza", I-00185 Rome, Italy
 - 35 Nuclear Physics Institute, St. Petersburg, Russia
 - 36 University and INFN, Salerno, I-84100 Salerno, Italy
 - 37 University of California, San Diego, CA 92093, USA
 - 38 Dept. de Física de Partículas Elementales, Univ. de Santiago, E-15706 Santiago de Compostela, Spain
 - 39 Bulgarian Academy of Sciences, Central Lab. of Mechatronics and Instrumentation, BU-1113 Sofia, Bulgaria
 - 40 Center for High Energy Physics, Adv. Inst. of Sciences and Technology, 305-701 Taejon, Republic of Korea
 - 41 University of Alabama, Tuscaloosa, AL 35486, USA
 - 42 Utrecht University and NIKHEF, NL-3584 CB Utrecht, The Netherlands
 - 43 Purdue University, West Lafayette, IN 47907, USA
 - 44 Paul Scherrer Institut, PSI, CH-5232 Villigen, Switzerland
 - 45 DESY-Institut für Hochenergiephysik, D-15738 Zeuthen, FRG
 - 46 Eidgenössische Technische Hochschule, ETH Zürich, CH-8093 Zürich, Switzerland
 - 47 University of Hamburg, D-22761 Hamburg, FRG
 - 48 National Central University, Chung-Li, Taiwan, China
 - 49 Department of Physics, National Tsing Hua University, Taiwan, China
- § Supported by the German Bundesministerium für Bildung, Wissenschaft, Forschung und Technologie
‡ Supported by the Hungarian OTKA fund under contract numbers T019181, F023259 and T024011.
¶ Also supported by the Hungarian OTKA fund under contract numbers T22238 and T026178.
‡ Supported also by the Comisión Interministerial de Ciencia y Tecnología.
Also supported by CONICET and Universidad Nacional de La Plata, CC 67, 1900 La Plata, Argentina.
‡ Supported by Deutscher Akademischer Austauschdienst.
◇ Also supported by Panjab University, Chandigarh-160014, India.
△ Supported by the National Natural Science Foundation of China.
† Deceased.

Table 1: The number of expected signal (SIG), background (BG) events and observed candidates (DATA) for the $\sqrt{s} = 189$ GeV data after a cut on the final discriminant corresponding to a signal-over-background ratio greater than 0.05. The number of signal events includes cross-efficiencies from other signal channels, events from fusion processes, charm and gluonic Higgs decays. Events are uniquely assigned to a channel.

Selection		Mass hypothesis								
		$m_H = 85$ GeV			$m_H = 90$ GeV			$m_H = 95$ GeV		
H	Z	SIG	BG	DATA	SIG	BG	DATA	SIG	BG	DATA
$b\bar{b}$	$q\bar{q}$	21.2	73.3	78	17.6	78.4	90	8.6	53.7	51
$b\bar{b}$	$\nu\bar{\nu}$	9.0	21.3	22	5.9	16.0	17	2.3	9.2	4
$b\bar{b}$	e^+e^-	1.8	3.0	3	1.2	3.5	1	0.6	2.3	1
$b\bar{b}$	$\mu^+\mu^-$	1.7	5.5	5	1.1	3.0	3	0.5	1.9	1
$b\bar{b}$	$\tau^+\tau^-$	0.7	1.2	0	0.4	0.8	0	0.2	0.5	0
$\tau^+\tau^-$	$q\bar{q}$	1.6	5.0	3	1.1	4.0	3	0.4	2.4	2

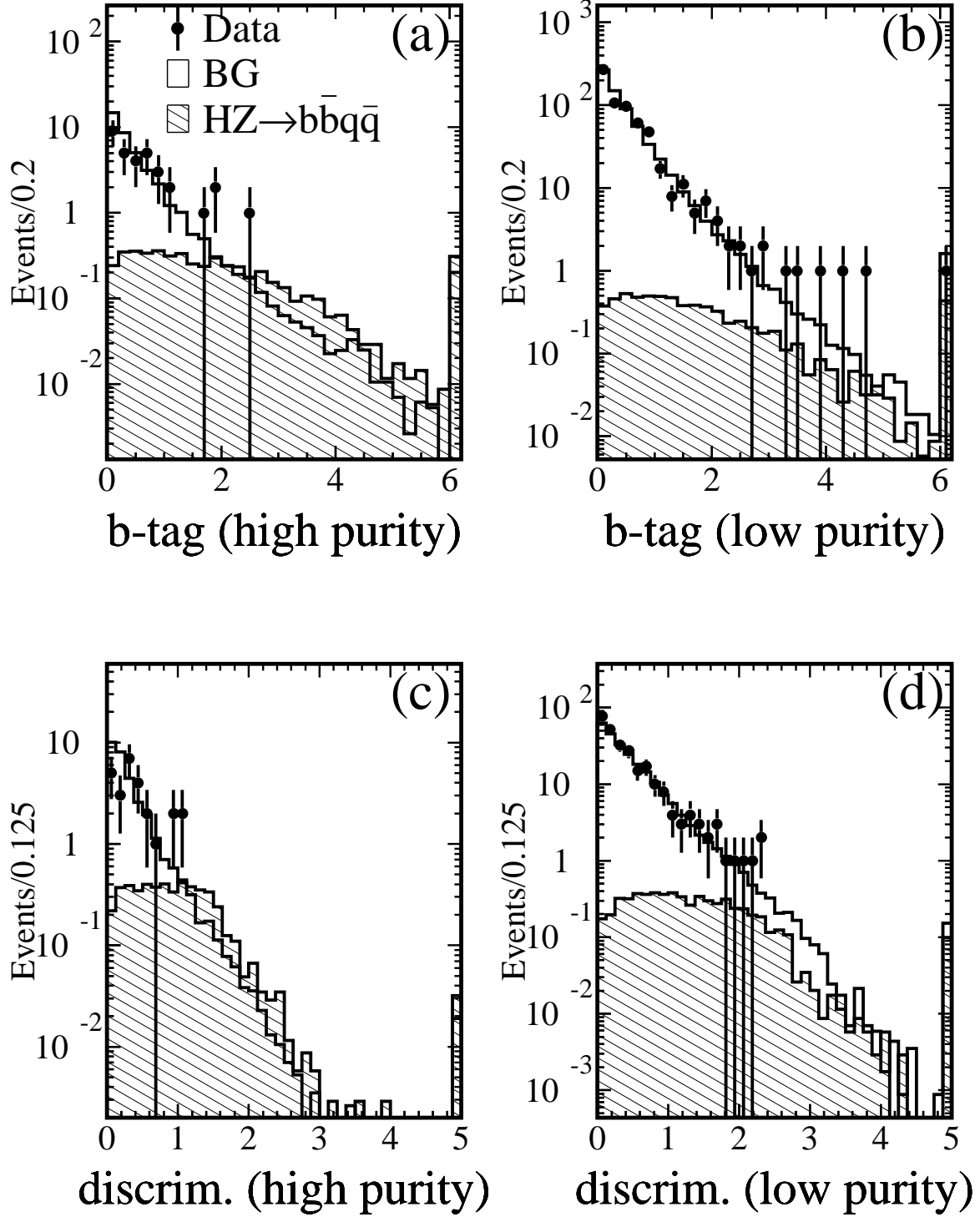


Figure 1: The b-tag distributions for the (a) high purity and (b) low purity analyses, and the final discriminant for the (c) high purity and (d) low purity analyses of $HZ \rightarrow b\bar{b}q\bar{q}$. The points are the 189 GeV data, the open histograms are Monte Carlo background and the hatched histograms are the Higgs signal. The signal is shown for $HZ \rightarrow b\bar{b}q\bar{q}$ with $m_H = 95$ GeV and is normalized to the number of expected events. The last bin in each histogram contains the overflows.

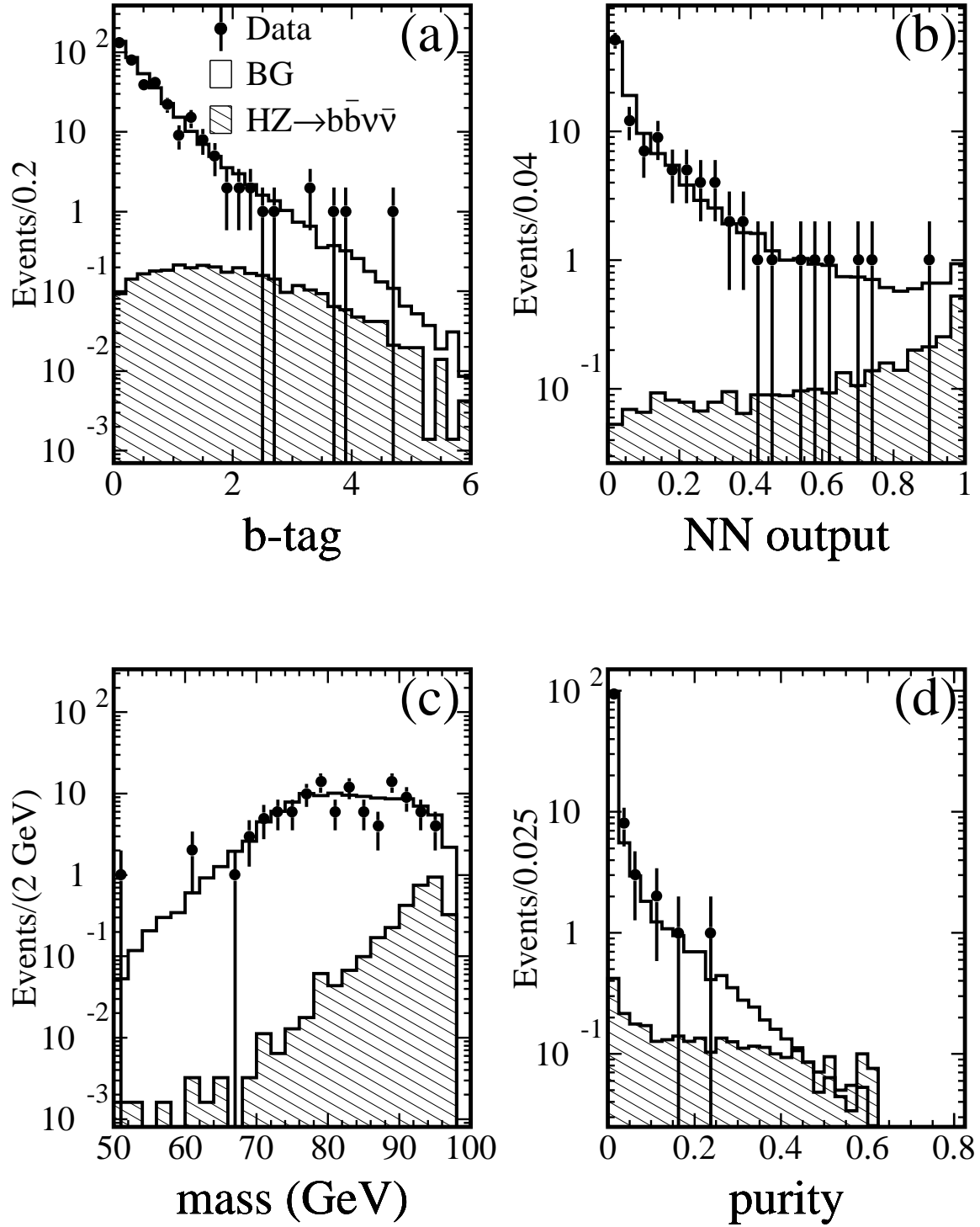


Figure 2: Distributions of the (a) b-tag, (b) neural network output, (c) hadronic mass, M_H^{5C} , and (d) purity variable for the $HZ \rightarrow b\bar{b}\nu\bar{\nu}$ analysis. The points are the 189 GeV data, the open histograms the background and the hatched histograms are for $HZ \rightarrow b\bar{b}\nu\bar{\nu}$ with $m_H = 95$ GeV, normalized to the number of expected events.

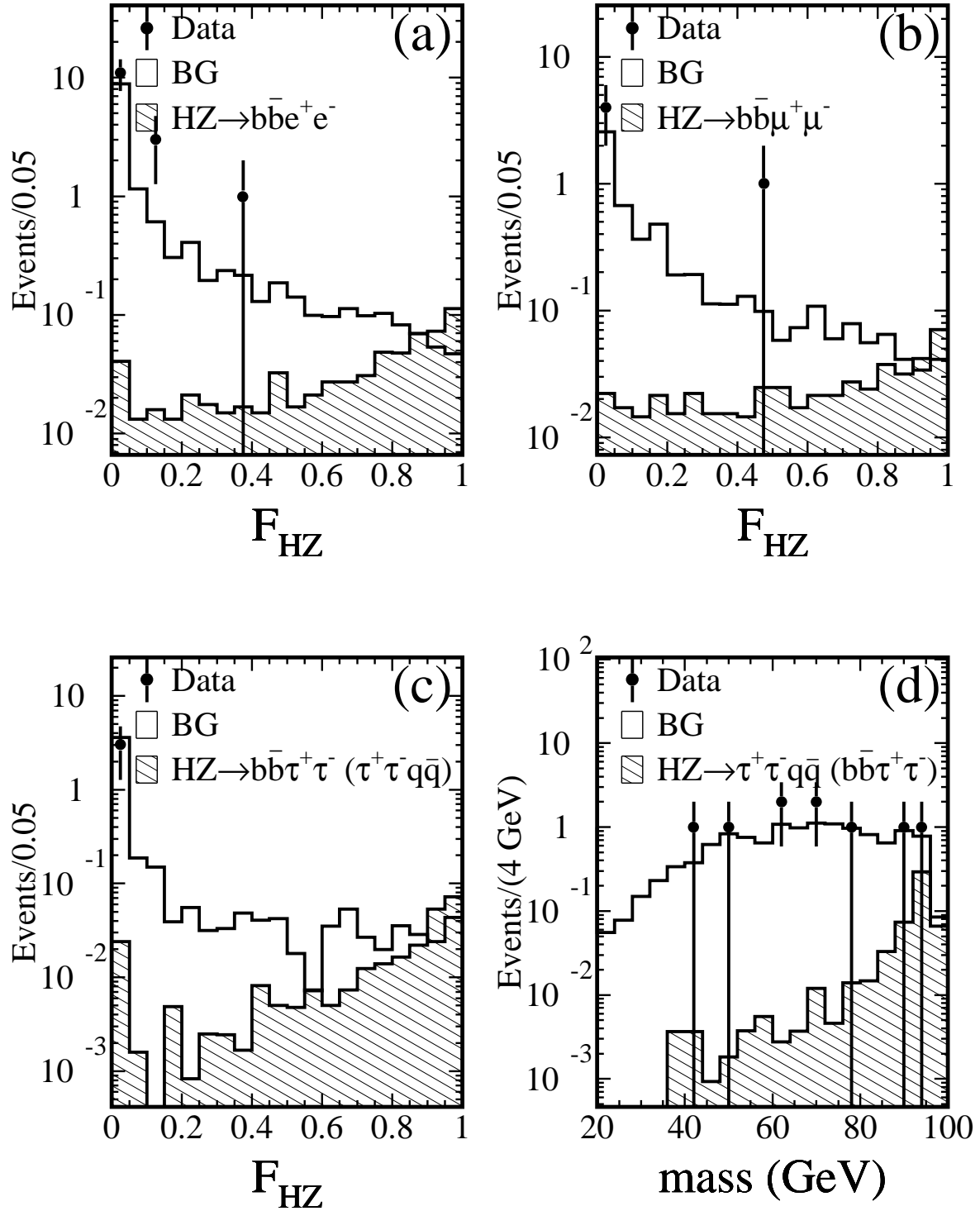


Figure 3: Distributions of the final discriminant for the (a) $\text{HZ} \rightarrow b\bar{b}e^+e^-$, (b) $\text{HZ} \rightarrow b\bar{b}\mu^+\mu^-$, (c) $\text{HZ} \rightarrow b\bar{b}\tau^+\tau^-$ and (d) $\text{HZ} \rightarrow \tau^+\tau^-q\bar{q}$ channels for the 189 GeV data, background and a Higgs signal of 95 GeV, normalized to the number of expected events. The signal events in the $\text{HZ} \rightarrow b\bar{b}\tau^+\tau^-$ and $\text{HZ} \rightarrow \tau^+\tau^-q\bar{q}$ plots include the branching-ratio-corrected cross-efficiencies for these channels. Events are uniquely assigned to only one of these channels.

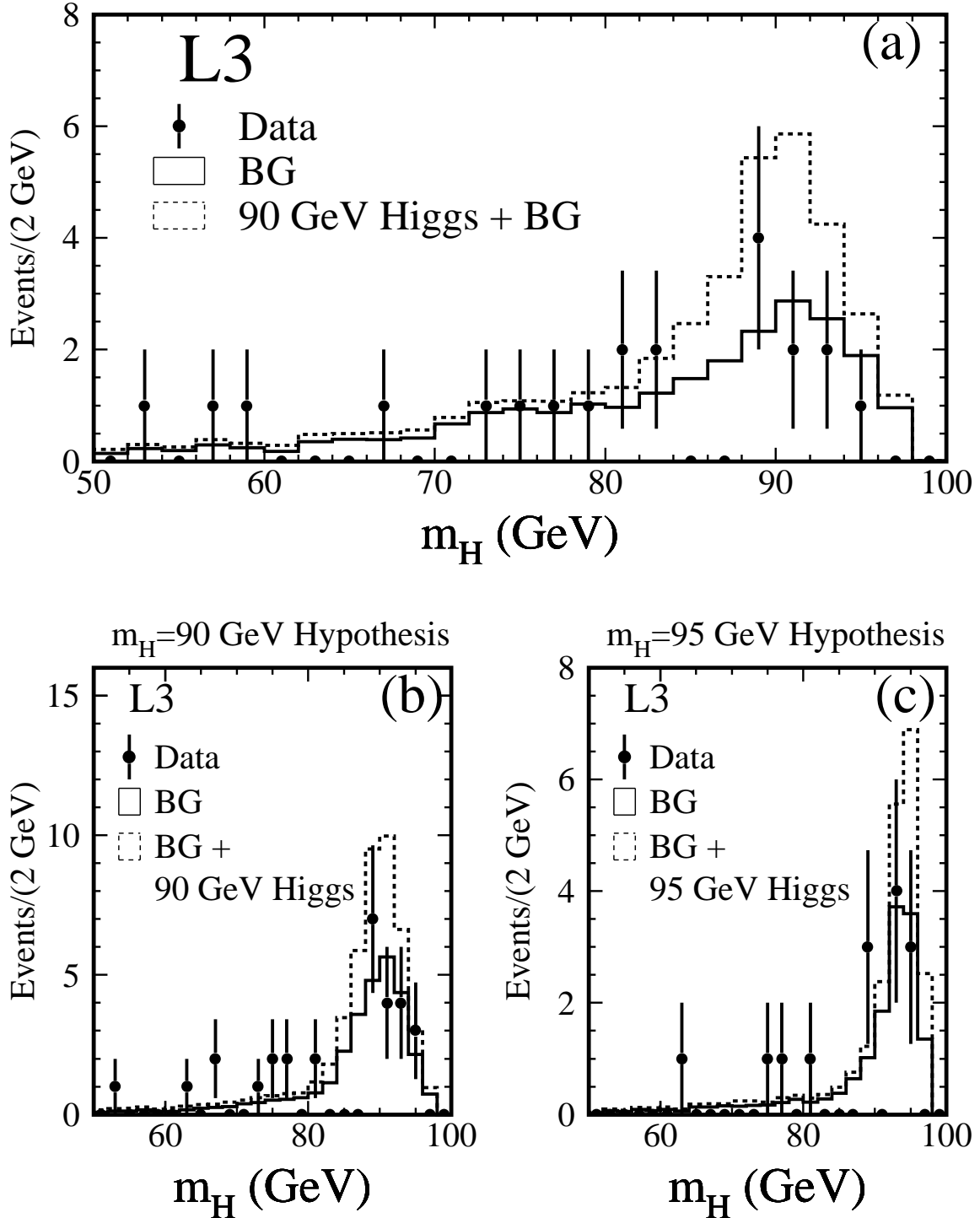


Figure 4: Reconstructed Higgs mass distributions in the 189 GeV data for the most significant signal-like events of the various analyses: (a) after mass-independent cuts on b-tag or neural network output to select candidates; (b-c) after cuts on the final discriminant (signal-over-background ratio greater than 0.25) for the mass hypothesis (b) $m_H = 90$ GeV and (c) $m_H = 95$ GeV. In all plots, the points are the data, the solid histograms are the Monte Carlo background and the dashed histograms are the Monte Carlo background plus Higgs signal.

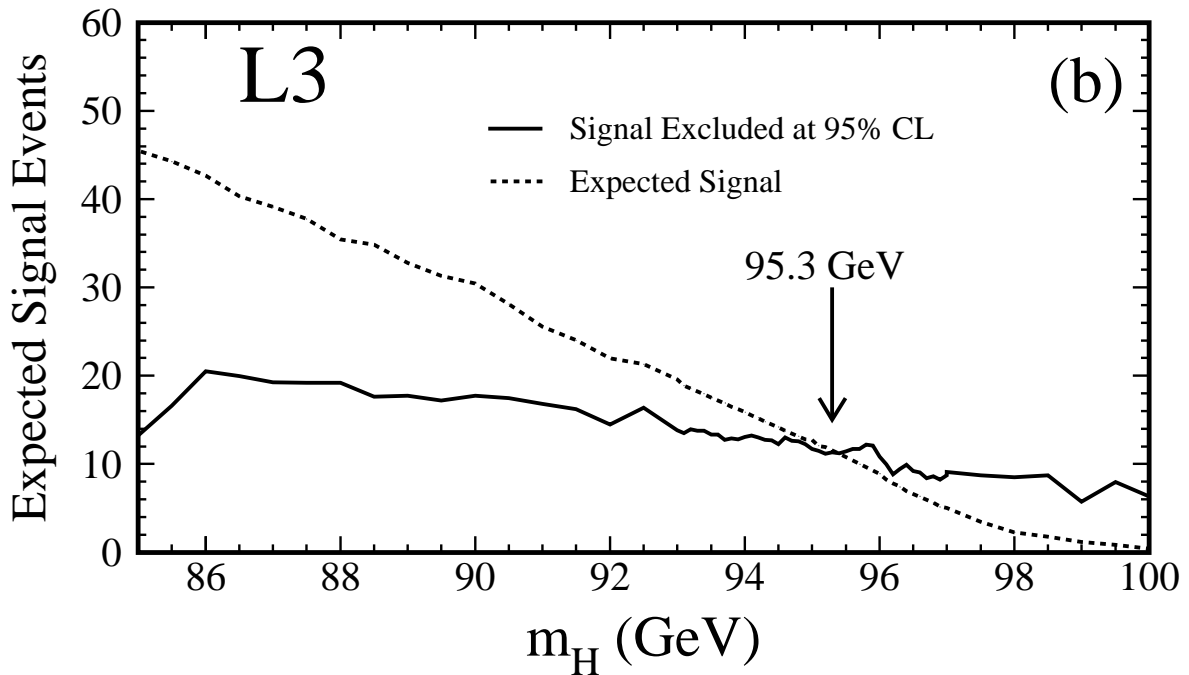
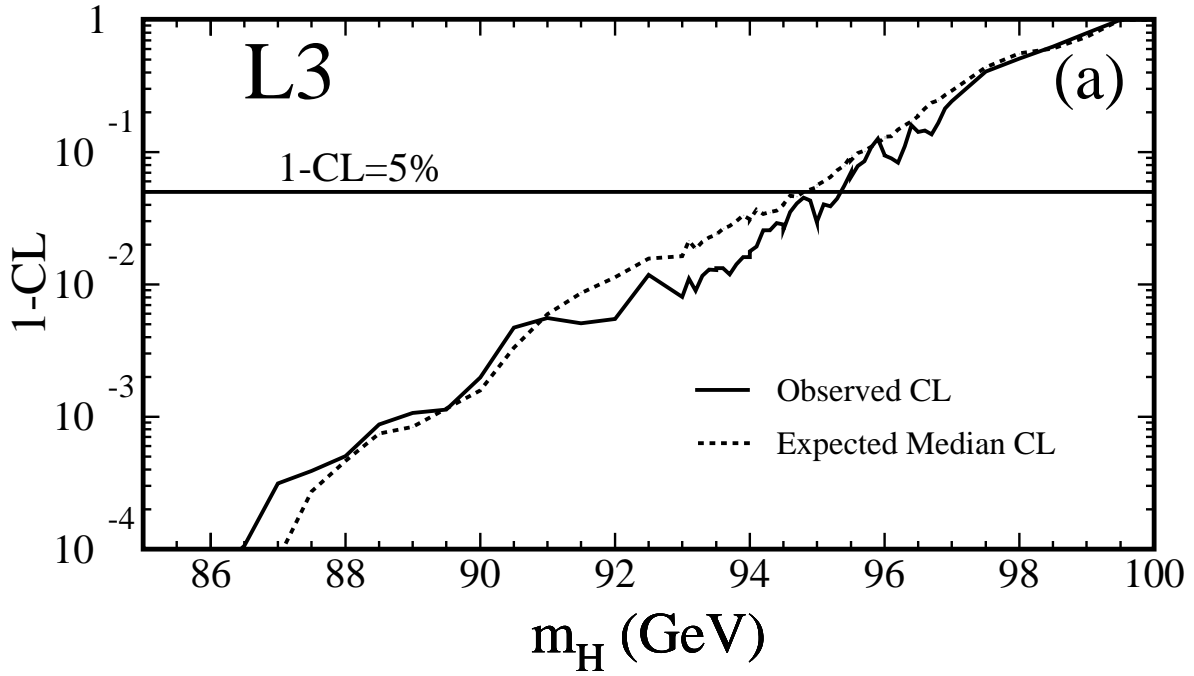


Figure 5: (a) The observed and expected median confidence levels as a function of the Higgs mass. (b) The number of expected and excluded signal events. Both plots include results from lower center-of-mass energies. The lower limit on the Higgs mass is set at $m_H > 95.3$ GeV at the 95% CL.